Wireless Power Transmission Based on Sandwiched Composite Piezoelectric Transducers in Length Extensional Vibration

Shuyu Lin, Hui Cao, and Xiaoyang Qiao

***Abstract*—A new type of wireless power transmission system is proposed. It is composed of two sandwiched composite piezoelectric transducers in length extensional vibration, which are connected together by an intermediate metal transmission cylinder. When the dielectric and mechanical losses are considered, the resonance/antiresonance frequency equations are obtained. The effect of the mechanical and the dielectric loss, the geometrical dimension and the load electric impedance on the effective electromechanical coupling coefficient, the voltage gain, and the power ratio is analyzed. It is shown that the mechanical and the dielectric losses almost have no effect on the resonance/antiresonance frequency. The geometrical dimension has obvious effect on the resonance/antiresonance frequency, the voltage gain, the effective electromechanical coupling coefficient and the power ratio. Corresponding to definite geometrical dimensions, the effective electromechanical coupling coefficient and the voltage gain have maximum values. There is optimum load electric impedance at which the power ratio reaches the maximum value. Two wireless power transmission systems are designed and manufactured; the resonance/antiresonance frequencies, the voltage gain, and the power ratio are measured. It is shown the measured frequencies are in good agreement with the theoretical results.**

***Index Terms*—Effective electromechanical coupling coefficient, longitudinal vibration, power ratio, resonance frequency, sandwiched composite piezoelectric transducer, voltage gain, wireless power transmission.**

I. Introduction

WIRELESS power or energy transmission is the transmission of electrical energy from a power source to an electrical load without man-made conductors. Wireless power transmission is useful in cases where interconnecting wires are inconvenient, hazardous, or impossible [1]–[3]. The problem of wireless power transmission differs from that of wireless telecommunications, such as radio. In the latter, the proportion of energy received becomes critical only if it is too low for the signal to be distinguished from the background noise. With wireless power transmission, efficiency is the more significant parameter. A large part of the energy sent out by the generating plant must arrive at the receivers to make the system economical. Nowadays, the means by which wireless power transmission can be realized are mainly based on the electromagnetic induction method [4] and the electromagnetic resonance induction method [5]–[10]. Other methods under consideration are electromagnetic radiation in the form of microwaves or lasers [11]–[18]. Ultrasonic waves are also used for the wireless power transmission [19]–[21], where the ultrasonic wave is first generated by an ultrasonic transducer or generator, and then the wave propagates through air or solid medium and received by a piezoelectric receiver and finally converted into electric energy. In recent years, piezoelectric devices are also used in power electronics and energy conversion [22]–[27]. In these applications, the piezoelectric devices are mainly used as piezoelectric transformers or actuators.

In this paper, the wireless power transmission system based on the longitudinally composite sandwiched piezoelectric ceramic transducers is theoretically and experimentally studied. When the mechanical and dielectric losses are considered, the dependence of the electromechanical characteristics on the geometrical dimension and the load electric impedance is analyzed. It is shown that the analytical resonance frequencies are in good agreement with the experimental results.

In the fields of wireless power transmission, almost all related transmission systems are based on the electromagnetic induction method and the electromagnetic resonance induction method. Wireless power transmission based on ultrasonic method is also proposed and studied. In the previous wireless power transmission systems based on ultrasonic method, air is generally chosen as the transmission medium. Because of the high ultrasonic absorption and the nonlinear effect of high-power ultrasound in the air, the transmission power, and the distance are limited. In this paper, the wireless power transmission system based on the longitudinally sandwiched piezoelectric transducers is first proposed. This is a kind of new energy transmission structure. In this structure, the power transmission is based on the piezoelectric effect, and a solid metal cylinder is chosen as the transmission medium. Since the energy transmission system is a kind of resonance structure, its transmission efficiency is high. On the other hand, the nonlinear effect in the system is less than that in the air; therefore, the transmission power can be high. It is estimated that the transmission power can reach as high as several hundreds of watts, and the energy transmission distance can reach as far as about several meters.

Manuscript received February 5, 2015; revised August 3, 2015 and September 8, 2015; accepted November 11, 2015. Date of publication November 20, 2015; date of current version March 25, 2016. This work was supported by the National Natural Science Foundation of China (11174192, 11374200) and the Research Fund for the Doctoral Program of Higher Education of China (Grant No 2011020211010). Recommended for publication by Associate Editor M. A. E. Andersen.

The authors are with the Shaanxi Key Laboratory of Ultrasonics, Applied Acoustics Institute, Shaanxi Normal University, Xian, Shaanxi 710062, China (e-mail: sylin@snnu.edu.cn; caohui@snnu.edu.cn; xyqiao@snnu.edu.cn).

Color versions of one or more of the figures in this paper are available online at http://ieeexplore.ieee.org.

Digital Object Identifier 10.1109/TPEL.2015.2502586

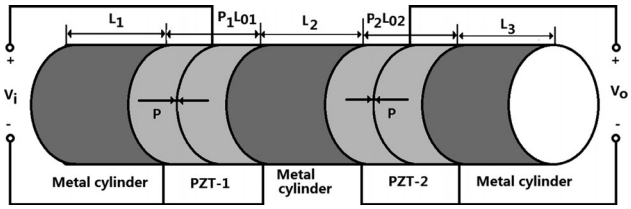

Fig. 1. Three-dimensional diagram of a longitudinally composite piezoelectric ceramic wireless power transmission system.

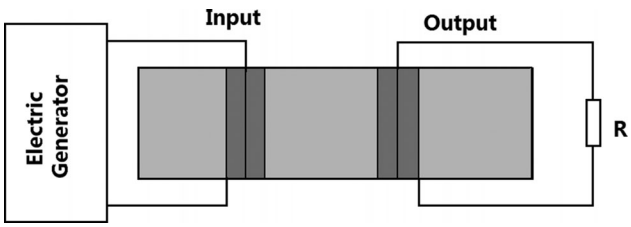

Fig. 2. Working Circuit diagram for a wireless power transmission system.

II. Theoretical Analysis on the Electromechanical Characteristics

Fig. 1 illustrates the three-dimensional diagram of a longitudinally composite piezoelectric ceramic wireless power transmission system. It consists of two longitudinally polarized piezoelectric ceramic stacks, the intermediate mechanical transmission cylinder, and the front and back end metal masses that are clamped together by a central high-strength metal bolt or high strength glue. In the figure, the arrow *P* represents the polarization direction of the piezoelectric ceramic ring. In Fig. 1, the length of the back-end mass, the mechanical transmission cylinder, and the front-end mass are L_1, L_2, and L_3. There are P_1 and P_2 pieces of piezoelectric disks or rings in the input and output piezoelectric ceramic stacks, the thickness for each ring is L_{01} and L_{02}. r_1, r_2, r_3 and r_{01}, r_{02} are the radius of the end mass, the mechanical transmission cylinder, and the piezoelectric ceramic stacks. In the present case, $r_1 = r_2 = r_3 = r_{01} = r_{02}$.

The circuit diagram for a wireless power transmission system is shown in Fig. 2. In practical applications, the input end of the system is electrically excited by an electric generator; the output end is loaded and connected by an electric resistance. Its working principle is explained as follows: when the input piezoelectric stack is excited by an external electric signal, longitudinal vibration will be produced by means of the converse piezoelectric effect. The longitudinal vibration then propagates through the intermediate transmission cylinder and arrives at the output piezoelectric ceramic stack. By means of the direct piezoelectric effect, the longitudinal vibration is converted to electric signal in the output piezoelectric stack, and at its output electric terminals, the different loads can be excited electrically and the required power can be produced in the loads.

Based on the electromechanical equivalent circuit of the longitudinally composite piezoelectric transducer [28]–[30], the electromechanical equivalent circuit of the wireless power transmission system can be obtained as shown in Fig. 3. In the figure, $\mathrm{V_i}$ is the input voltage and $\mathrm{V_o}$ is the output voltage. R represents the load electric resistance. R_m represents the mechanical loss between the contacting surfaces of the piezoelectric ceramic

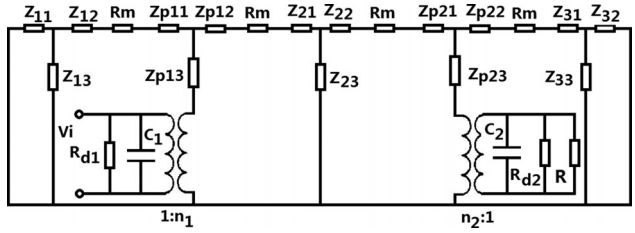

Fig. 3. Electromechanical equivalent circuit of a longitudinally composite piezoelectric wireless power transmission system.

stack and the mechanical transmission cylinder. In practical cases, the bulk mechanical loss in the system cannot be ignored, especially when the system is operated on high-exciting voltage. However, the bulk mechanical loss in the system is difficult to formulate and, therefore, accurate analytical theory is difficult to find. Therefore, the effect of the bulk mechanical loss will be studied in future work. R_{d1} and R_{d2}, C_1 and C_2, n_1 and n_2 are the dielectric loss, the clamped capacitance, and the electromechanical conversion coefficient of the piezoelectric ceramic stacks. Their expressions are as follows:

$$C_1 = P_1\varepsilon_{33}^{\mathrm{T}}(1-K_{33}^2)S_{01}/L_{01},$$
$$C_2 = P_2\varepsilon_{33}^{\mathrm{T}}(1-\mathrm{K}_{33}^2)S_{02}/L_{02} \quad (1)$$

$$n_1 = d_{33}S_{01}/(\mathrm{s}_{33}^{\mathrm{E}}L_{01}), n_2 = \mathrm{d}_{33}S_{02}/(\mathrm{s}_{33}^{\mathrm{E}}L_{02}) \quad (2)$$

$$R_{\mathrm{d1}} = R_{\mathrm{e1}}/P_1, \quad R_{\mathrm{d2}} = R_{\mathrm{e2}}/P_2 \quad (3)$$

where R_{e1} and R_{e2} are the dielectric loss of each piezoelectric ceramic element. S_{01} and S_{02} are the cross-sectional areas. $S_{01} = \pi r_{01}^2$, $S_{02} = \pi r_{02}^2$. When the material and the geometrical dimensions of the piezoelectric ceramic elements in the input and output piezoelectric stack are the same, we have $R_{\mathrm{e1}} = R_{\mathrm{e2}} = R_e$. $\varepsilon_{33}^{\mathrm{T}}$,$K_{33}$,$\mathrm{d}_{33}$ and $\mathrm{s}_{33}^{\mathrm{E}}$ are the dielectric constant, the electromechanical coupling coefficient, the piezoelectric constant, and the elastic compliance constant of the piezoelectric material. In Fig. 3, the expressions for the series and parallel impedances are as follows [31]–[32]:

$$Z_{11} = Z_{12} = jZ_1\tan(\frac{\mathrm{k}_1L_1}{2}),\ Z_{13} = \frac{Z_1}{j\sin(\mathrm{k}_1L_1)} \quad (4)$$

$$Z_{21} = Z_{22} = jZ_2\tan(\frac{\mathrm{k}_2L_2}{2}),\ Z_{23} = \frac{Z_2}{j\sin(\mathrm{k}_2L_2)} \quad (5)$$

$$Z_{31} = Z_{32} = jZ_3\tan(\frac{\mathrm{k}_3L_3}{2}),\ Z_{33} = \frac{Z_3}{j\sin(\mathrm{k}_3L_3)} \quad (6)$$

$$Z_{P11} = Z_{P12} = jZ_{01}\tan(p_1\mathrm{k}_0L_{01}/2),$$
$$Z_{P13} = \frac{Z_{01}}{j\sin(p_1\mathrm{k}_0L_{01})} \quad (7)$$

$$Z_{P21} = Z_{P22} = jZ_{02}\tan(p_2\mathrm{k}_0L_{02}/2),$$
$$Z_{\mathrm{P23}} = \frac{Z_{02}}{j\sin(p_2\mathrm{k}_0L_{02})} \quad (8)$$

where $Z_1 = \rho_1c_1S_1, k_1 = \omega/c_1, c_1 = (E_1/\rho_1)^{1/2}, S_1 = \pi r_1^2, Z_2 = \rho_2c_2S_2, k_2 = \omega/c_2, c_2 = (E_2/\rho_2)^{1/2}, S_2 = \pi r_2^2, Z_3 = \rho_3c_3S_3, k_3 = \omega/c_3, c_3 = (E_3/\rho_3)^{1/2}, S_3 = \pi r_3^2\ \omega = 2\pi f$. In the present case, $r_1 = r_2 = r_3$. $Z_{01} = \rho_0c_0S_{01}, Z_{02} = \rho_0c_0$

$S_{02}, k_0 = \omega/c_0, c_0 = [1/(\mathrm{s}_{33}^{\mathrm{E}}\rho_0)]^{1/2}$.$\rho_1, \mathrm{E}_1$,$\rho_2, \mathrm{E}_2$ and ρ_3, E_3 are density and Young's modulus; c_1,c_2, c_3 and c_0 are sound speeds in the three metal cylinders and the piezoelectric material, respectively.

From Fig. 3, the parallel impedance of the clamped capacitance and the dielectric loss of the input and the output piezoelectric ceramic stack can be expressed as

$$Z_{c1} = \frac{R_{\mathrm{d}1}}{j\omega C_1 R_{\mathrm{d}1}+1} \tag{9}$$

$$Z_{c2} = \frac{R_{\mathrm{d}2}}{j\omega C_2 R_{\mathrm{d}2}+1}. \tag{10}$$

The reflected mechanical impedance of the output piezoelectric ceramic stack is

$$Z_{\mathrm{rm}} = n_2^2 \times \frac{Z_{c2} R}{Z_{c2} + R} \tag{11}$$

where *R* is the load electric resistance. When the contacting mechanical loss is considered, the input mechanical impedance of the front- and back-end metal masses can be obtained as

$$Z_{1m} = R_m + Z_{12} + \frac{Z_{11} Z_{13}}{Z_{11} + Z_{13}} \tag{12}$$

$$Z_{3m} = R_m + Z_{31} + \frac{Z_{32} Z_{33}}{Z_{32} + Z_{33}}. \tag{13}$$

The mechanical impedance at the contacting surface between the mechanical transmission cylinder and the output piezoelectric ceramic stack can be expressed as

$$Z_{p2} = R_m + Z_{p21} + \frac{(Z_{p23} + Z_{\mathrm{rm}})(Z_{p22} + Z_{3m})}{Z_{p22} + Z_{p23} + Z_{\mathrm{rm}} + Z_{3m}}. \tag{14}$$

The mechanical impedance at the contacting surface between the mechanical transmission cylinder and the input piezoelectric ceramic stack can be derived out

$$Z_{2m} = R_m + Z_{21} + \frac{Z_{23}(Z_{22} + Z_{p2})}{Z_{23} + Z_{22} + Z_{p2}}. \tag{15}$$

The equivalent mechanical impedance of the input piezoelectric ceramic stack can be obtained as

$$Z_m = Z_{p13} + \frac{(Z_{p12} + Z_{2m})(Z_{p11} + Z_{1m})}{Z_{p12} + Z_{p11} + Z_{2m} + Z_{1m}}. \tag{16}$$

The input electric impedance of the input piezoelectric ceramic stack, which is also the input electric impedance of the wireless power transmission system, can be obtained as

$$Z_{\mathrm{ie}} = R_{\mathrm{ie}} + jX_{\mathrm{ie}} = \frac{R_1 Z_m n_1^2}{j\omega C_1 (n_1^2 R_1 + Z_m) + R_1 Z_m} \tag{17}$$

where R_{ie} and X_{ie} are the input electric resistance and reactance. For a resonant piezoelectric device, when the imaginary part of the input electric impedance is equal to zero, the resonance frequency equation can be obtained

$$X_{\mathrm{ie}} = 0. \tag{18}$$

When the imaginary part of the input electric admittance, which is the reciprocal of the input electric impedance, is equal to zero, the antiresonance frequency equation is expressed as

$$\frac{X_{\mathrm{ie}}}{R_{\mathrm{ie}}^2 + X_{\mathrm{ie}}^2} = 0. \tag{19}$$

Based on (18) and (19), the resonance/antiresonance frequency can be calculated. However, it can be seen that these two equations are very complicated transcendental equations; they depend on the material parameters, the geometrical dimensions, the frequency and the vibrational modes of the system. When these related parameters are given, the resonance/antiresonance frequency can be obtained, and the effective electromechanical coupling coefficient k_{eff} can be computed according to the following equation:

$$k_{\mathrm{eff}}^2 = 1 - (\frac{\omega_r}{\omega_a})^2 \tag{20}$$

where $\omega_r = 2\pi f_r$, $\omega_a = 2\pi f_a$, f_r and f_a are the resonance/antiresonance frequency.

The voltage gain, which is defined as the ratio of the output voltage across the load electric impedance over the input voltage across the input piezoelectric ceramic stack, can be derived out from Fig. 3

$$G_v = \frac{V_o}{V_i} = \frac{R}{Z_{\mathrm{ie}}} \times \frac{1}{\mathrm{ZP}} \tag{21}$$

where ZP is a specific expression introduced for simplicity, its detailed expression is

$$\begin{aligned}\mathrm{ZP} = {} & (1 + \frac{Z_m}{n_1^2 Z_{c1}}) \times \frac{n_1}{n_2} \times \frac{Z_{p11} + Z_{1m} + Z_{p12} + Z_{2m}}{Z_{p11} + Z_{1m}} \\ & \times \frac{Z_{22} + Z_{23} + Z_{p2}}{Z_{23}} \times \frac{Z_{p22} + Z_{p23} + Z_{3m} + Z_{\mathrm{rm}}}{Z_{p22} + Z_{3m}} \\ & \times \frac{Z_{c2} + R}{Z_{c2}}.\end{aligned} \tag{22}$$

From (20) and (21), the effective electromechanical coupling coefficient and the voltage gain can be obtained.

The ratio of the output electric power over the input electric power, which is also defined as the efficiency, can be obtained as the following expressions:

$$G_p = \frac{P_o}{P_i} = \frac{V_o^2}{V_i^2} \times \frac{Z_{\mathrm{ie}}}{R} = R_v^2 \times \frac{Z_{\mathrm{ie}}}{R} \tag{23}$$

where Z_{ie} and R are the input electric impedance and the load electric resistance.

III. Numerical Simulation Analysis of the Performance Parameters

In Section II, the resonance frequency equation and the expressions for the effective electromechanical coupling coefficient, the voltage gain, and the power ratio are theoretically obtained. In order to optimize the performance of the system, the dependence of these characteristics on the working frequency, the geometrical dimensions, the mechanical and dielectric loss, and the load electric impedance are further studied. The material used for the end masses and the mechanical transmission cylinder is aluminum alloy, its material parameters are as follows:$\rho_1 = \rho_2 = \rho_3 = 2700\,\mathrm{kg/m^3}$, $\mathrm{E}_1 = E_2 = E_3 = 7.023 \times 10^{10}\,\mathrm{N/m^2}$. The piezoelectric ceramic stack is

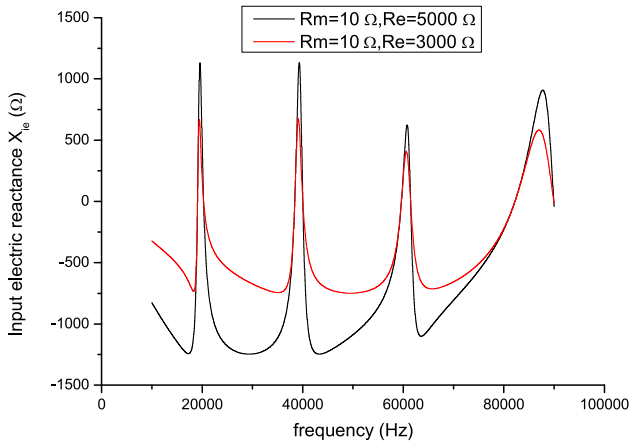

Fig. 4. Frequency response of the input electric reactance.

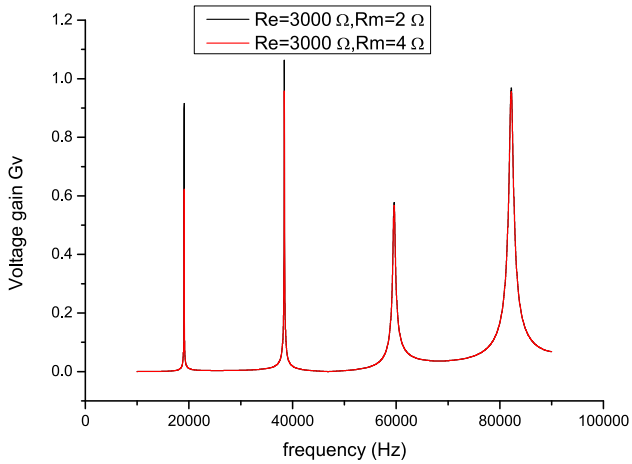

Fig. 5. Dependence of the voltage gain on the frequency.

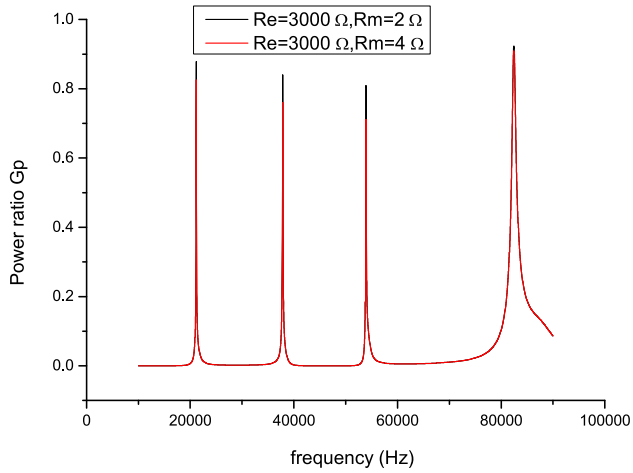

Fig. 6. Dependence of the power ratio on the frequency.

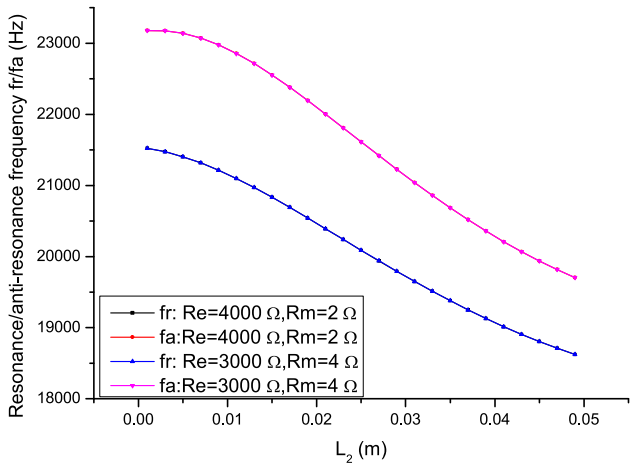

Fig. 7. Dependence of the resonance/antiresonance frequency on the geometrical dimensions under different mechanical and dielectric losses.

an equivalent of PZT-4. Its standard material properties are: $\rho_{01} = \rho_{02} = 7500\,\mathrm{kg/m^3}$, $s_{33}^{\mathrm{E}} = 15.5 \times 10^{-12}\mathrm{m^2/N}$, $K_{33} = 0.7$, $d_{33} = 496 \times 10^{-12} C/N$, $\varepsilon_0 = 8.8542 \times 10^{-12}\mathrm{F/m}$, $\varepsilon_{33}^{\mathrm{T}}/\varepsilon_0 = 1300$.

A. *Effect of the Mechanical and the Dielectric Loss on the Frequency Response*

When the material and the geometrical dimensions are determined, the dependence of the electromechanical parameters on the frequency can be obtained. Based on (17), (21), and (23), the frequency response of the input electric reactance, the voltage gain, and the power ratio are obtained as shown in Figs. 4–6. The geometrical dimensions are as follows: $L_1 = L_2 = 0.04\,\mathrm{m}$, $L_3 = 0.01\,\mathrm{m}$, $L_{01} = L_{02} = 0.006\,\mathrm{m}$, $r_1 = r_2 = r_3 = r_{01} = r_{02} = 0.01\,\mathrm{m}$, $p_1 = p_2 = 2$, the load electric resistance is $R = 50\,\Omega$.

From Fig. 4, three conclusions can be obtained. First, the longitudinally composite piezoelectric wireless power transmission system is a resonant device; there are many different vibrational modes. In the figure, different reactance peaks represent the different vibrational modes. Second, the mechanical and dielectric losses almost have no obvious effect on the resonance/antiresonance frequency. Third, the mechanical and dielectric losses affect the value of the input electric reactance. When the mechanical and dielectric losses are increased, the input electric reactance is decreased.

From Figs. 5 and 6, it can be seen that the voltage gain and the power ratio reach the maximum value near the resonance frequency. At different resonant modes, the maximum values of the voltage gain and the power ratio are different. When the losses are increased, the voltage gain and the power ratio are decreased.

B. *Effect of the Geometrical Dimensions on the Electromechanical Characteristics*

Based on the resonance frequency equation and the expressions of the voltage gain and the power ratio, the effect of the geometrical dimensions on the electromechanical characteristics are studied. Figs. 7–10 are the theoretically calculated relationship between the electromechanical parameters and the geometrical dimensions. In the analysis, the total length of the system is kept constant. The detailed dimensions are as follows: $L_1 = 0.04\,\mathrm{m}$, $L_2 + L_3 = 0.05\,\mathrm{m}$, $L_{01} = L_{02} = 0.006\,\mathrm{m}$, $r_1 = r_2 = r_3 = r_{01} = r_{02} = 0.01\,\mathrm{m}$, $p_1 = p_2 = 2$, the load electric resistance is $R = 50\,\Omega$. In this case, the variation of L_2 means that the position of the output piezoelectric

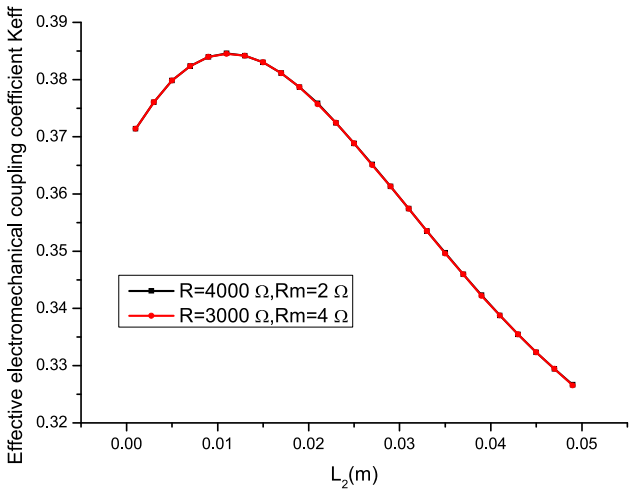

Fig. 8. Theoretical relationship between the effective electromechanical coupling coefficient and the geometrical dimensions.

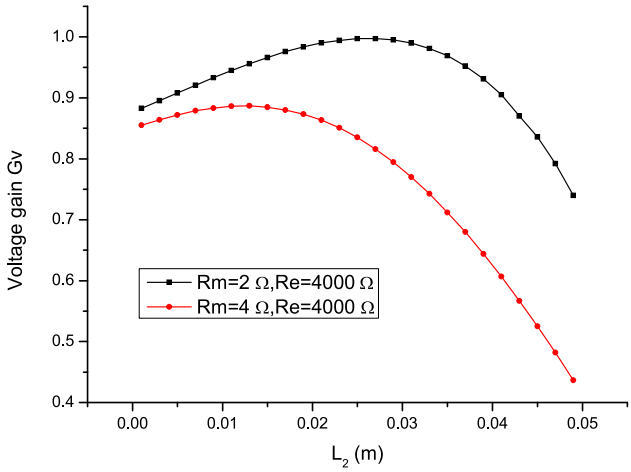

Fig. 9. Theoretical relationship between the voltage gain and the geometrical dimensions.

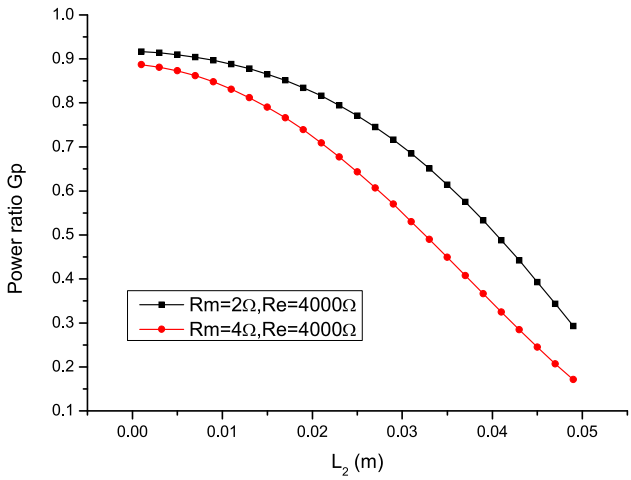

Fig. 10. Theoretical relationship between the power ratio and the geometrical dimensions.

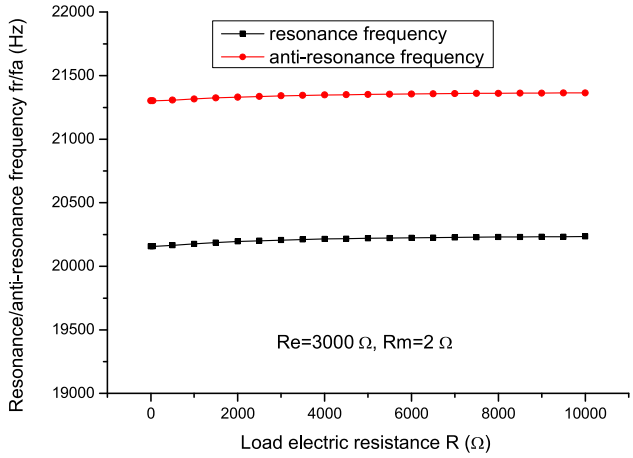

Fig. 11. Theoretical relationship between the resonance/antiresonance frequency and the load electric resistance.

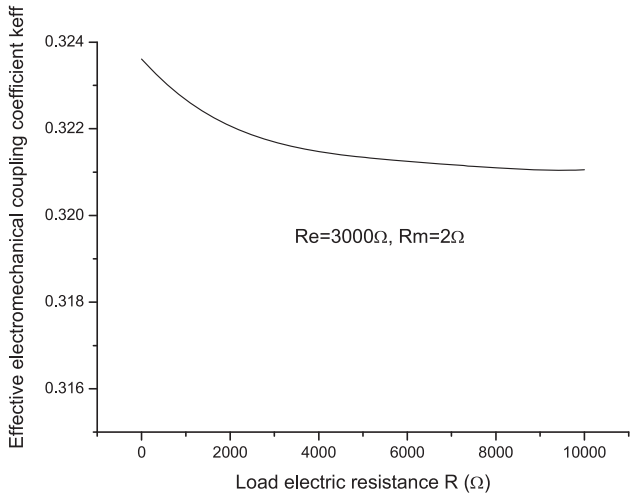

Fig. 12. Dependence of the effective electromechanical coupling coefficient on the load electric resistance.

ceramic stack is changed. When L_2 is increased, the output piezoelectric stack is away from the input piezoelectric stack. Fig. 7 describes the dependence of the resonance/antiresonance frequency on the geometrical dimensions when the mechanical and the dielectric losses are different. It can be seen that corresponding to different losses, the resonance/antiresonance frequency are almost the same. Therefore, it can be concluded that the mechanical and the dielectric losses have almost no effect on the resonance/antiresonance frequency of the system.

From the aforesaid results, it can be concluded that when the total length of the system is kept constant while the position of the output piezoelectric stack is changed, the electromechanical parameters are all changed. When the output piezoelectric stack is away from the input piezoelectric stack, the resonance/antiresonance frequency and the power ratio are decreased. At some definite dimensions, the effective electromechanical coupling coefficient and the voltage gain have maximum values. Therefore, by means of these analytical conclusions, the system performance can be optimized. On the other hand, it can be seen that the mechanical and dielectric losses almost have no effect on the resonance/antiresonance frequency

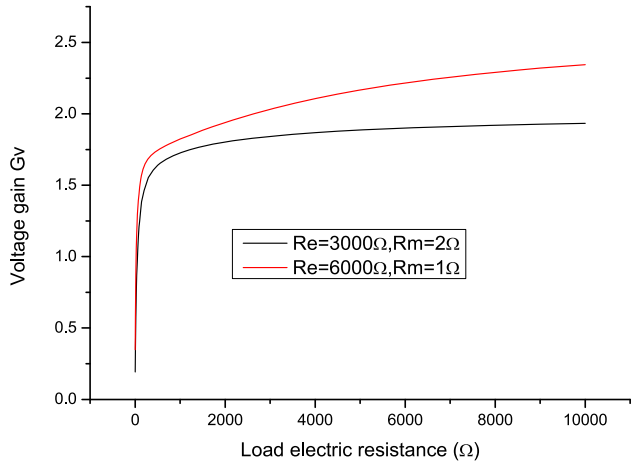

Fig. 13. Dependence of the voltage gain on the load electric resistance.

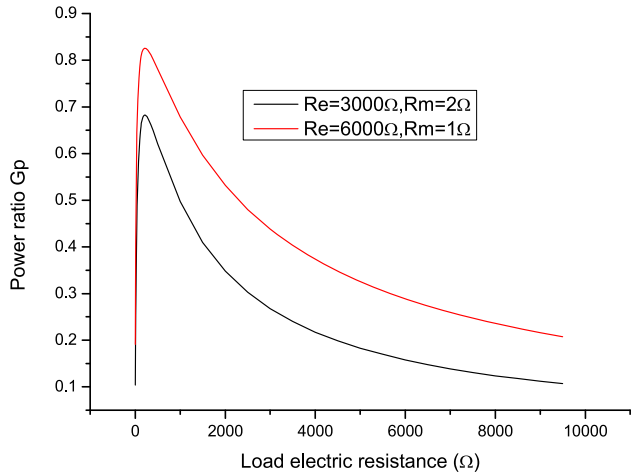

Fig. 14. Dependence of the power ratio on the load electric resistance of the system.

and the effective electromechanical coupling coefficient of the system. When the losses are increased, the voltage gain and the power ratio are decreased.

C. Dependence of the Electromechanical Characteristics on the Load Electric Resistance

It is well known that the load of any device affects its performance. In this section, the load dependence is theoretically analyzed. The geometrical dimensions are all specified as follows: $L_1 = L_2 = 0.04$ m, $L_3 = 0.01$ m, $L_{01} = L_{02} = 0.005$ m, $r_1 = r_2 = r_3 = r_{01} = r_{02} = 0.01$ m, $p_1 = p_2 = 2$. The load electric resistance R is changed.

Figs. 11–14 are the theoretical relationship between the electromechanical parameters and the load electric resistance. It can be seen that the load electric resistance almost has no effect on the resonance/antiresonance frequency. When the load electric resistance is increased, the effective electromechanical coupling coefficient is slightly decreased and the voltage gain is increased. There is an optimum load electric resistance at which the power ratio reaches the maximum value.

On the other hand, it can be seen that when the load electric resistance is small, the voltage gain and the power ratio are increased rapidly. When the load electric resistance is increased to some extent, the voltage gain is increased slowly; the power ratio reaches the maximum value and then is decreased. When the mechanical and dielectric losses are increased, the voltage gain and the power ratio are both decreased.

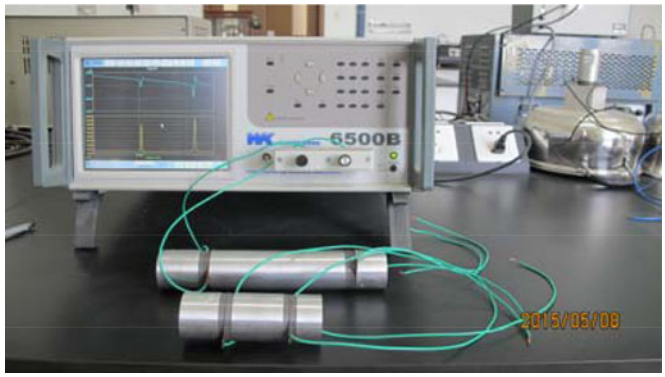

Fig. 15. Photograph of the frequency measurement setup of a wireless power transmission system.

In this section, the relationship between the electromechanical characteristics and the working frequency, the geometrical dimensions, and the load electric resistance is theoretically analyzed and some conclusions are obtained. By means of properly choosing the geometrical dimensions and the load electric resistance, the optimization design of the longitudinally composite piezoelectric ceramic wireless power transmission system can be realized and its performance can be improved.

IV. Experiments

To verify the aforesaid theoretical analysis, two wireless power transmission systems are designed and manufactured. The materials are the same as those in the aforesaid analysis and the standard material parameters are used in the design. The geometrical dimensions are listed in Table I. The resonance/antiresonance frequencies, the voltage gain, and the power ratio are measured in the following sections.

A. Measurement of the Resonance/Antiresonance Frequencies

The resonance/antiresonance frequencies are measured by using 6500B Precision Impedance Analyzer made by Wayne Kerr Electronics of West Sussex in U.K. as shown in Fig. 15. The analytical and experimental resonance/antiresonance frequencies of the system are listed in Tables II and III. In these tables, f_r and f_a are the analytical resonance/antiresonance frequencies; $f_{\rm mr}$ and $f_{\rm ma}$ are the measured results. $\Delta_1 = |f_r - f_{\rm mr}|/f_{\rm mr}, \Delta_2 = |f_a - f_{\rm ma}|/f_{\rm ma}$. For simplicity, only two limiting load cases are considered, one is short circuited and the other is open circuited.

From the aforesaid results, it can be seen that the analytical resonance/antiresonance frequencies are in good agreement with the experimental results, especially for the first vibrational mode. The error between the analytical and the experimental results may be caused by the following factors: first, the mechanical and dielectric losses used in the analytical theory are different from those in the real systems; second, the standard material parameters are used in the theoretical calculation, how-

TABLE I
GEOMETRICAL DIMENSIONS OF THE PIEZOELECTRIC WIRELESS POWER TRANSMISSION SYSTEMS

No.	L_1(mm)	L_2(mm)	L_3(mm)	L_{01}(mm)	L_{02}(mm)	p_1	p_2	$r_1 = r_2 = r_3$(mm)	$r_{01} = r_{02}$(mm)
1	30	40	20	5	5	2	2	19.5	19.0
2	30	130	40	5	5	2	2	19.5	19.0

TABLE II
ANALYTICAL AND EXPERIMENTAL RESONANCE/ANTI-RESONANCE FREQUENCIES OF THE SYSTEMS WITH DIFFERENT LOAD ELECTRIC RESISTANCES AT THE FIRST VIBRATIONAL MODE

No.	$R(\Omega)$	f_r(Hz)	f_{mr}(Hz)	Δ_1(%)	f_a(Hz)	f_{ma}(Hz)	Δ_2(%)
1	0	20 288	19 548	3.78	20 914	20 050	4.31
	∞	21 316	20 050	6.31	21 661	20 553	5.39
2	0	10 484	10 276	2.02	10 576	10 402	1.67
	∞	10 547	10 276	2.64	10 774	10 402	3.58

TABLE III
ANALYTICAL AND EXPERIMENTAL RESONANCE/ANTIRESONANCE FREQUENCIES OF THE SYSTEMS WITH DIFFERENT LOAD ELECTRIC RESISTANCES AT THE SECOND VIBRATIONAL MODE

No.	$R(\Omega)$	f_r(Hz)	f_{mr}(Hz)	Δ_1(%)	f_a(Hz)	f_{ma}(Hz)	Δ_2(%)
1	0	43 807	39 648	10.5	46 071	41 156	11.9
	∞	47 043	41 658	12.9	49 740	43 165	15.2
2	0	22 364	22 211	0.69	22 913	22 462	2.01
	∞	22 971	22 588	1.70	23 872	22 965	3.95

Fig. 16. Experimental setup for the measurement of the voltage gain.

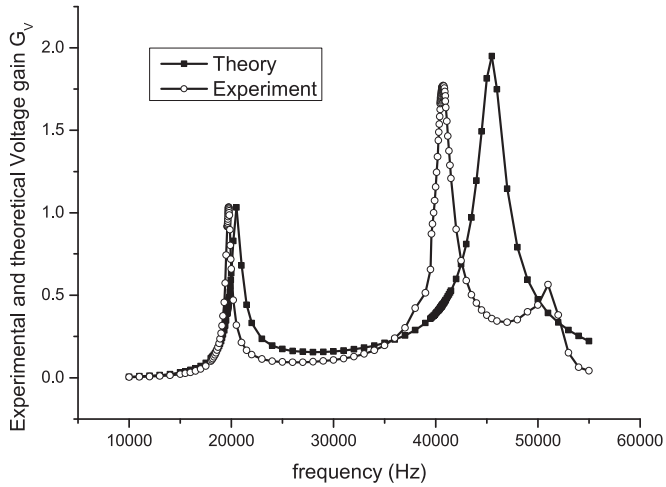

Fig. 17. Measured frequency response of the voltage gain of a wireless power transmission system.

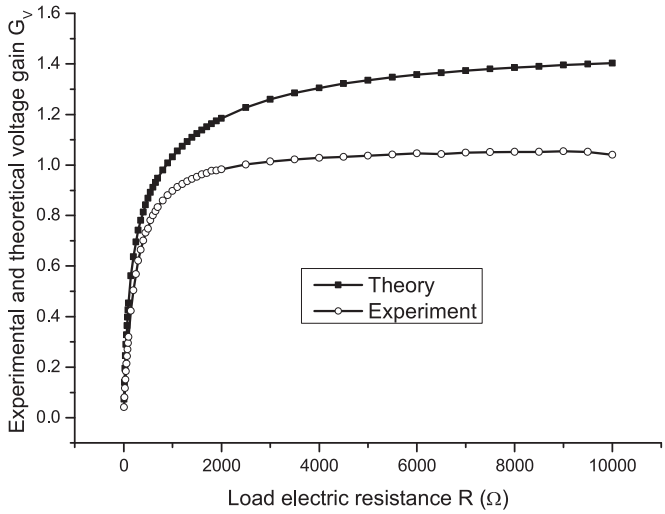

Fig. 18. Measured load dependence of the voltage gain of a wireless power transmission system.

ever, the real material parameters are more or less different from the standard material parameters; and third, in the present theoretical analysis, one-dimensional analytical theory is assumed, it is required that the radial dimension should be much less than the wavelength. For the second vibrational mode, the resonance frequency is higher than that of the first vibrational mode, and the corresponding longitudinal wavelength is decreased. In this case, the radius is not much less than the wavelength. Therefore, the systematic error is produced to some extent.

B. Measurement of the Voltage Gain of the Systems

The voltage gain of a wireless power transmission system (No.1) is measured by using the experimental setup as shown in Fig. 16. In the figure, Arbitrary Function Generator is used to electrically excite the system; its output voltage and frequency are changeable. Two digital multimeters are used to measure the input and the output voltages. A variable electric resistance is used as the electric load resistance. Based on the experimental setup, the frequency response of the voltage gain is measured as shown in Fig. 17. In the measurement of the frequency response of the voltage gain, the load electric resistance is kept at $R = 1000\ \Omega$. The peak-to-peak value of the output voltage of the Arbitrary Function Generator is 20 V and no power amplifier is used. Meanwhile, the dependence of the voltage gain on the load electric resistance is also measured as shown in Fig. 18. For comparison, the theoretically calculated results are also shown

Fig. 19. Experimental setup for the measurement of the power ratio.

in these figures. In the numerical simulation, the mechanical and the electric losses of the system are chosen as follows: $R_e = 20\,000\ \Omega, R_m = 95\ \Omega$.

From the measured and theoretical results, it can be seen that the measured variation tendency of the voltage gain with the frequency and the load electric resistance is basically in agreement with the theoretical results. There is some error between the measured and the theoretical absolute values of the voltage gain. The reason for this error can be explained as follows: first, the mechanical and the dielectric losses used in the theoretical analysis are difficult to determine, and they are more or less different from the real losses in the real systems; second, in the theoretical analysis, the standard material parameters are used, they are more or less different from the real material parameters; and third, in the theoretical analysis, the exciting circuit of the system is not considered and, therefore, it is assumed that the voltage across the system is unchanged. In the experiment, however, the function generator used has a definite output resistance. Since the wireless power transmission system is a resonant device, when the frequency is changed, its input electric impedance is correspondingly changed, and therefore, the voltage across the system is also changed. In this case, the frequency response of the input electric impedance may be changed because of the different voltages across the system, and therefore, some error may be caused.

It should be pointed out that in the measurement of the frequency response and load dependence of the voltage gain and the power gain, no power amplifier is used. Since the Arbitrary Function Generator is a signal source of low voltage and power, the measurement results and the variation tendency only reflect the characteristics of the system at low signal. It is well known that under the conditions of high voltage and power, the system characteristics are different. For example, the mechanical and the dielectric losses will increase, and therefore, the power gain and the voltage gain of the system will decrease.

C. Measurement of the Power Ratio of a Wireless Power Transmission System

The power ratio of the system (No.1) is measured by using the experimental setup as shown in Fig. 19. In this section, two experiments are done. First, the dependence of the power ratio on the load electric resistance at the resonance frequency of the system is measured and the results are shown in Fig. 20. The experimental setup for the measurement of the dependence of

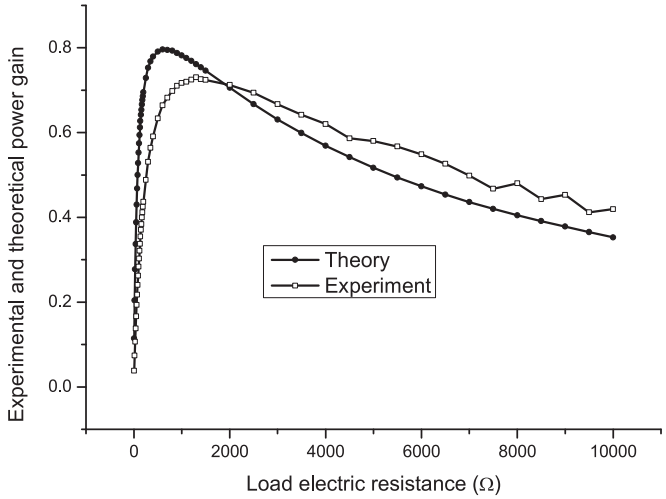

Fig. 20. Measured load dependence of the power ratio at resonance.

TABLE IV
MEASURED POWER RATIO OF A TRANSMISSION SYSTEM AT HIGH INPUT ELECTRIC POWER

P_0 (W)	1.1	4.5	8.8	18.9	36.0	38.1	38.0	41.0	42.0
P_i (W)	3.0	13.4	25.6	53.1	96.4	101.1	109.2	124.1	126.3
G_{Pm}	0.37	0.34	0.34	0.36	0.37	0.38	0.35	0.33	0.33
G_P	0.39	0.39	0.39	0.39	0.39	0.39	0.39	0.39	0.39

the power ratio on the load electric resistance is composed of a DG 1022U Function/Arbitrary Waveform Generator, a WT 1600 two channel digital power meter, and a variable resistance box of low signal. In the experiment, the electric signal frequency of the DG 1022U Function/Arbitrary Waveform Generator is kept at 19 560 Hz, which is approximately equal to the resonance frequency of the system. The peak-to-peak value of the output voltage of the generator is 20 V. Since no amplifier is used, the measurement results only reflect the characteristics of the system at low signal of voltage and power. For comparison, the theoretical dependence of the power gain on the load electric resistance is calculated and shown in Fig. 20. In the calculation, the same mechanical and the electric losses of $R_e = 20\,000\ \Omega, R_m = 95\,\Omega$ are used. It can be seen that the experimental results are basically in agreement with the theoretical curve. It is considered that the error is mainly caused by the mechanical and the dielectric loss of the system. Second, the power transmission performance of the system under the condition of high-input electric power is measured. In the experiment, an AG 1012 Amplifier of T&C power conversion, Inc. is used to amplify the output voltage signal of the function generator. The variable resistance box of low signal is substituted by a high-power electric resistance of $50\ \Omega$. At the resonance frequency of the system, the power ratio is measured at different input electric power. The measured results are listed in Table IV. In the table, P_0 and P_i are the measured output and input power of the transmission system, G_{Pm} is the experimental power ratio. For comparison, the theoretical power ratio of the system at low level of exciting electric voltage when the load electric resistance is $50\ \Omega$ is also given in the table. In the calculation of the power gain, the mechanical and the electric losses of $R_e = 20\,000\ \Omega, R_m = 95\,\Omega$ are used. In the experiment, the peak-to-peak value of the output voltage of the Function/Arbitrary Waveform Generator is kept at

1 V. The output voltage of the power amplifier is changed from several volts to about 100 V.

From the experimental results of the system at high-power level, it can be seen that the power ratio at high-power level is lower than that at the low-power level and the power gain measurement error is comparatively large at high-power level. The reasons can be explained as following: first, under high-exciting electric power, the loss of the system is increased, and the performance of the system is affected; second, the resonance frequency is affected by the high-exciting electric voltage, and it is difficult for the system to be at resonance; and third, when test time goes on, the system becomes heated and its performance becomes unstable.

Based on the aforesaid theoretical analysis and experimental results, it can be seen that the power gain of the system depends on the load electric resistance and the input electric power level. At a definite load electric resistance, the power gain can reach a maximum value, and this electric resistance can be defined as the matched resistance. On the other hand, the power gain depends on the input electric power level. At low-power level, the power gain of the system can reach as high as about 0.9. When the power level is increased, the power gain is decreased because of the heating and instability of the system. In order to maintain high-power gain and stable working of the system, some necessary measures should be taken. First, the system must be kept at the resonance state by means of the automatic frequency tracking. Second, appropriate cooling measures should be taken, such as the wind cooling or the water cooling. When these measures are efficiently used, the power gain of the system can reach as high as about 0.7; the power level can reach as high as several hundreds of watts.

In practical applications, the exciting circuit of the system should have the function of frequency automatic tracking. In this case, when the resonance frequency of the system is changed, the frequency of the output electric signal of the amplifier will keep the same as the resonance frequency of the transmission system.

In practical applications, the input and output voltage and power of the system in working condition depend on the performance of the longitudinally sandwiched piezoelectric transducers and the load electric resistance. Nowadays, the input electric voltage of the transducer can reach as high as several hundreds of volts, and the input electric power for a single piezoelectric transducer can reach as high as several hundreds of watts depending on the load electric resistance. It should be pointed out that under the condition of high-exciting voltage and power, the exciting circuit of the system should have the function of frequency automatic tracking, and the system should be cooled by taking some measures in order to keep stable and reliable work.

The potentially general applications of the system include two respects. One is for the power transmission in some severe environments, where the electric supply is difficult and impossible. For example, to ensure the reliability of nuclear stockpiles, there have been proposals that piezoelectric transducers are used to generate acoustic waves propagating through a sealed armor for transmitting a small amount of power to the electronic devices inside the armor. This structure is also expected to be used in some periodically recharging batteries to power electronic devices operating in some sealed and hazardous environments into which the physical access is prohibited. Meanwhile, it may also be used for wireless power transmission in some complex mechanical machinery. The other applications are for the voltage conversion. In the second case, the system can be regarded and used as a high-power piezoelectric transformer.

V. Conclusion

A new type of wireless power transmission systems based on sandwiched longitudinal composite piezoelectric ceramic transducers is proposed and studied. The frequency equations are obtained. The relationship between the resonance/antiresonance frequency, the effective electromechanical coupling coefficient, the voltage gain and the power ratio with the frequency, the geometrical dimensions and the load electric impedance is analyzed. The resonance/antiresonance frequencies, the voltage gain, and the power ratio are measured. To sum up the above analysis, the following conclusions can be drawn.

1) The sandwiched longitudinal composite piezoelectric ceramic wireless power transmission system is a kind of resonant device; it has many different vibrational modes. At the resonance frequency, the voltage gain and the power ratio reach the maximum values. Depending on the different applications, the system may be operated on different vibrational modes.
2) The mechanical and dielectric losses almost have no effect on the resonance/antiresonance frequency and the effective electromechanical coupling coefficient. However, other electromechanical characteristics are dependent on the losses. When the mechanical and dielectric losses are increased, the input electric impedance, the voltage gain, and the power ratio are decreased.
3) When the total length of the system is kept constant, the position of the output piezoelectric stack has obvious effect on the electromechanical characteristics. When the output piezoelectric stack is moved away from the input piezoelectric stack, the resonance/antiresonance frequency and the power ratio are decreased; the effective electromechanical coupling coefficient and the voltage gain have maximum values corresponding to some definite geometrical dimensions.
4) When the load electric resistance is increased, the resonance/antiresonance frequencies are slightly increased and the effective electromechanical coupling coefficient is slightly decreased. The voltage gain is increased; there is an optimum load electric resistance at which the power ratio reaches the maximum value.
5) The dielectric and mechanical losses in the system are difficult to calculate and measure quantitatively. Moreover, they depend on the level of the electric signal and the mechanical vibration. To improve the performance of the system, the losses should be kept as low as possible. This can be realized by choosing the materials with low loss and improving the mechanical manufacturing process of the system.
6) In the theoretical analysis, the exciting circuit of the system is not considered. It is assumed that the exciting circuit of the system is an ac voltage source with constant amplitude. In practical applications, the function generator or power amplifier has a definite output resistance; its output voltage is not constant and dependent on the input electric impedance of the wireless power transmission systems.

REFERENCES

[1] K. Shenai, "Power electronics module: Enabling the 21st-century energy economy," *IEEE Power Electron. Mag.*, vol. 1, no. 3, pp. 27–32, Sep. 2014.

[2] J. M. Miller, O. C. Onar, C. White, S. Campbell, C. Coomer, L. Seiber, R. Sepe, and A. Steyerl, "Demonstrating dynamic wireless charging of an electric Vehicle: The benefit of electrochemical capacitor smoothing," *IEEE Power Electron. Mag.*, vol. 1, no. 1, pp. 12–24, Mar. 2014.

[3] K. Chen and Z. Zhao, "Analysis of the double-layer printed spiral coil for wireless power transfer," *IEEE J. Emerg. Sel. Topics Power Electron.*, vol. 1, no. 2, pp. 114–121, Jun. 2013.

[4] J. J. Hirai, T. W. Kim, and A. Kawamura, "Wireless transmission of power and information for cableless linear motor drive," *IEEE Trans. Power Electron.*, vol. 15, no. 1, pp. 21–27, Jan. 2000.

[5] A. Karalis, J. Joannopoulos, and M. Soljacic, "Wireless nonradiative energy transfer," *Arxiv Preprint Phys.*, vol. 0611063, pp. 1–17, 2006.

[6] A. Kurs, A. Karalis, R. Moffatt, J. D. Joannopoulos, P. Fisher, and M. Soljacic, "Wireless power transfer via strongly coupled magnetic resonance," *Science*, vol. 317, pp. 83–86, Jul. 6, 2007.

[7] A. Karalis, J. D. Joannopoulos, and M. Soljacic, "Efficient wireless nonradiative mid-range energy transfer," *Annal. Phys.*, vol. 4, pp. 45–56, 2007.

[8] R. E. Hamam, A. Karalis, J. Joannopoulos, and M. Soljačić, "Efficient weakly-radiative wireless energy transfer: An EIT-like approach," *Annal. Phys.*, vol. 324, no. 8, pp. 1783–1795, 2009.

[9] F. Zhang, S. A. Hackworth, and C. Li, "Relay effect of wireless power transfer using strongly coupled magnetic resonances," *IEEE Trans. Magn.*, vol. 47, no. 5, pp. 1478–1481, May 2011.

[10] M. Soljačić, A. Kurs, A. Karalis, R. Moffatt, J. D. Joannopoulos, and P. Fisher, "Wireless power transfer via strongly coupled magnetic resonances," *Sci. Exp.*, vol. 112, no. 6, pp. 1–10, 2007.

[11] B. Corey and S. Jeremy, "A space-to-space microwave wireless power transmission experiential mission using small satellites," *Acta Astronautica*, vol. 103, pp. 193–203, Oct./Nov. 2014.

[12] E. Bou, E. Alarcon, A. Saenz-Otero, and C. Mandy, "Translayer optimized co-design of in-space microwave based wireless power transfer," in *Proc. IEEE Int. Symp. Circuits Syst.*, May 30, 2010/Jun. 2, 2010, pp. 885–888.

[13] J. Benford, "Space applications of High-Power microwaves," *IEEE Trans. Plasma Sci.*, vol. 36, no. 3, pp. 569–581, Jun. 2008.

[14] N. Shinohara and K. Hashimoto, "Microwave power transmission technologies for SPS," *Shinku/J. Vacuum Soc. Japan*, vol. 51, no. 8, pp. 513–518, 2008.

[15] R. B. Vaganov, I. P. Korshunov, and E. N. Korshunova, "Selection of the microwave-beam parameters in a wireless system for energy transportation from a space electric power station to the Earth," *J. Commun. Technol. Electron.*, vol. 53, no. 2, pp. 195–198, 2008.

[16] H. Matsumoto, "Research on solar power station and microwave power transmission in Japan: Review and perspectives," *IEEE Microw. Mag.*, vol. 3, no. 4, pp. 36–45, Dec. 2002.

[17] T. Blackwell, "Recent demonstrations of laser power beaming at DFRC and MSFC," in *Proc. AIP Conf. Proc.: Beamed Energy Propulsion. 3d Int. Symp. Beamed Energy Propulsion*, 2005, pp. 73–85.

[18] F. Steinsiek, K. H. Weber, W. P. Foth, H. J. Foth, and C. Schafer, "Wireless power transmission technology development and demonstrations," in *Proc. 2nd Int. Conf. Recent Adv. Space Technol.*, 2005, pp. 140–149.

[19] I. Toshihiko, K. Yasuyuki, and O. Junichi, "Impact of a wireless power transmission system using an ultrasonic air transducer for low-power mobile applications," in *Proc. IEEE Ultrason. Symp.*, 2003, pp. 1368–1371.

[20] H. Hu, Y. Hu, C. Chen, and J. Wang, "A system of two piezoelectric transducers and a storage circuit for wireless energy transmission through a thin metal wall," *IEEE Trans. Ultrasonics, Ferroelectrics, Frequency Control*, vol. 55, no. 10, pp. 2312–2319, Oct. 2008.

[21] N. K. Hoang, L. Jeong-Seon, and L. Sang-Gug," Maximum power transfer considering limited available input power in ultrasonic wireless power transfer for implanted medical devices," in *Proc. IEEE 4th Int. Conf. Consumer Electron.*, 2014, pp. 431–432.

[22] A. Denisov and E. M. Yeatman, "Micromechanical actuators driven by ultrasonic power transfer," *J. Microelectromechan. Syst.*, vol. 23, no. 3, pp. 750–759, 2014.

[23] B. Ducharne, L. Garbuio, M. Lallart, D. Guyomar, G. Sebald, and J. Y. Gauthier, "Nonlinear technique for energy exchange optimization in piezoelectric actuators," *IEEE Trans. Power Electron.*, vol. 28, no. 8, pp. 3941–3948, Aug. 2013.

[24] M. S. Roedgaard, M. Weirich, and M. A. E. Andersen, "Forward conduction mode controlled piezoelectric transformer-based PFC LED drive," *IEEE Trans. Power Electron.*, vol. 28, no. 10, pp. 4841–4849, Oct. 2013.

[25] A. Romani, M. Filippi, and M. Tartagni, "Micropower design of a fully autonomous energy harvesting circuit for arrays of piezoelectric transducers," *IEEE Trans. Power Electron.*, vol. 29, no. 2, pp. 729–739, Feb. 2014.

[26] V. A. Klymko, M. A. M. Hendrix, J. L. Duarte, and E. Lomonova, "Efficient waveform preservation of discrete spectrum signals with multilayered piezoelectric transformer," *IEEE Trans. Power Electron.*, vol. 29, no. 8, pp. 4382–4391, Aug. 2014.

[27] J. Sankman and D. Ma, "A 12-μW to 1.1-mW AIM piezoelectric energy harvester for Time-Varying vibrations with 450-nA IQ," *IEEE Trans. Power Electron.*, vol. 30, no. 2, pp. 632–643, Feb. 2015.

[28] S. Lin, "Load characteristics of high power sandwich piezoelectric ultrasonic transducers," *Ultrasonics*, vol. 43, no. 5, pp. 365–373, 2005.

[29] S. Lin, "Analysis of multifrequency langevin composite ultrasonic transducers," *IEEE Trans. Ultrasonics, Ferroelectrics, Frequency Control*, vol. 56, no. 9, pp. 1990–1998, Sep. 2009.

[30] S. Lin and C. Xu, "Analysis of the sandwich ultrasonic transducer with two sets of piezoelectric elements," *Smart Mater. Struct.*, vol. 17, no. 6, pp. 1–9, 2008.

[31] Z. M. Lin, *Principle and Design of Ultrasonic Concentrators*. Beijing, China: Science Press, 1987, pp. 36–38.

[32] S. Y. Lin, *Principle and design of ultrasonic transducers*. Beijing, China: Science Press, 2004, pp. 91–111.

Shuyu Lin was born in Shandong Province, China, on December 22, 1962. He received the Eng.D. degree from the Tokyo Institute of Technology, Tokyo, Japan, in September 2002.

He is currently a Professor and the Director of Applied Acoustics Institute, Shaanxi Normal University, Shaanxi, China. His current research interests include high-power ultrasonics, piezoelectric transducers and resonators, piezoelectric transformer and motors, and different ultrasonic applications. He has published more than 100 papers. His current research fields focus on radially sandwiched piezoelectric ultrasonic transducer, high-power cylindrical ultrasonic transducer, and piezoelectric transformer.

Dr. Lin is currently a Fellow and Administrator of the Acoustical Society of China, Director of power ultrasonics committee of the Acoustical Society of China.

Hui Cao received the B.Sc. degree in electrical engineering from the Nanjing University of Science and Technology, China, in 1991, and the M.S. and Ph.D. degrees from the Institute of Applied Acoustics, Shaanxi Normal University, Shaanxi, China, in 1998 and 2004, respectively.

He is currently an Associate Professor with the School of Physics & Information Technology, Shaanxi Normal University. His current research interests include ultrasonic transducer, signal processing, and biological effect.

Xiaoyang Qiao received the B.Sc. degree in physics from the Tianjin Normal University, Tianjin, China. She is currently working toward the graduate degree in the Institute of Applied Acoustics, Shaanxi Normal University, Xi'an, China.

Her current research interest includes acoustic cavitation.